Published in final edited form as:
Chemistry. 2012 May 21; 18(21): 6555–6567. doi:10.1002/chem.201102829.

Electronic Structure Analysis of the Oxygen-Activation Mechanism by Fe^{II}- and α-Ketoglutarate (αKG)-Dependent Dioxygenases

Shengfa Ye[a], **Christoph Riplinger**[a], **Andreas Hansen**[a], **Carsten Krebs**[b], **J. Martin Bollinger Jr.**[b], and **Frank Neese**[*,a]

[a] Max-Plank Institute for Bioinorganic Chemistry Stiftstrasse 34–36 45470 Mülheim an der Ruhr (Germany)

[b] Department of Chemistry Department of Biochemistry and Molecular Biology The Pennsylvania State University University Park, Pennsylvania 16802 (USA)

Abstract

α-Ketoglutarate (αKG)-dependent nonheme iron enzymes utilize a high-spin (HS) ferrous center to couple the activation of oxygen to the decarboxylation of the cosubstrate αKG to yield succinate and CO_2, and to generate a high-valent ferryl species that then acts as an oxidant to functionalize the target $C–_H$ bond. Herein a detailed analysis of the electronic-structure changes that occur in the oxygen activation by this enzyme was performed. The rate-limiting step, which is identical on the septet and quintet surfaces, is the nucleophilic attack of the distal O atom of the O_2 adduct on the carbonyl group in αKG through a bicyclic transition state (^{5,7}TS1). Due to the different electronic structures in ^{5,7}TS1, the decay of ^{7}TS1 leads to a ferric oxyl species, which undergoes a rapid intersystem crossing to form the ferryl intermediate. By contrast, a HS ferrous center ligated by a peroxosuccinate is obtained on the quintet surface following ^{5}TS1. Thus, additional two single-electron transfer steps are required to afford the same Fe^{IV}–oxo species. However, the triplet reaction channel is catalytically irrelevant. The biological role of αKG played in the oxygen-activation reaction is dual. The αKG LUMO (C=O π*) serves as an electron acceptor for the nucleophilic attack of the superoxide monoanion. On the other hand, the αKG HOMO ($C1–_{C2}$ σ) provides the second and third electrons for the further reduction of the superoxide. In addition to density functional theory, high-level ab initio calculations have been used to calculate the accurate energies of the critical points on the alternative potential-energy surfaces. Overall, the results delivered by the ab initio calculations are largely parallel to those obtained with the B3LYP density functional, thus lending credence to our conclusions.

Keywords

ab initio calculations; density functional calculations; electronic structure; enzymes; O–O activation

*Fax: (+49)208-306-3951 frank.neese@mpi-mail.mpg.de.

Supporting information for this article is available on the WWW under http://dx.doi.org/10.1002/chem.201102829.

Introduction

The Fe^{II}- and α-ketoglutarate (αKG)-dependent dioxygenases constitute the largest class of mononuclear nonheme iron enzymes and catalyze a broad range of pivotal metabolic transformations. For example, these enzymes are involved in many important biochemical processes such as degradation of xenobiotics,[1] synthesis of antibiotics and collagen,[2] repair of DNA and RNA bases,[3] control of oxygen homeostasis,[4] and regulation of gene expression.[5] The most studied and prototypical member of the αKG-dependent enzyme family is taurine (2-aminoethane-1-sulfonic acid)/αKG dioxygenase (TauD),[6] which enables *Escherichia coli* to use the aliphatic sulfonate taurine as a sulfur source during periods of sulfate starvation.[7]

It is commonly assumed that all Fe^{II}- and αKG-dependent dioxygenases utilize a common mechanism, which was initially proposed by Hanauske-Abel and Günzler for prolyl-4-hydroxylase (P4H)[8] (Scheme 1). This mechanism involves 1) binding of the cosubstrate αKG to the high-spin (HS) ferrous center in a bidentate fashion; 2) binding of substrate in the vicinity of the active site, which causes dissociation of the remaining water ligand from the Fe^{II} site; 3) addition of oxygen to the quaternary enzyme/Fe^{II}/αKG/substrate complex to yield intermediate **I**, a $\{FeO_2\}^8$ complex in which O_2 is proposed to bind in an end-on mode to the iron center; 4) nucleophilic attack of the uncoordinated O atom on the C2 atom of αKG to form a bicyclic intermediate **II**; 5) decarboxylation of αKG and cleavage of the O–O bond, which leads to formation of a high-valent Fe^{IV}–oxo intermediate III, concurrent with release of CO_2; 6) cleavage of the target C–H bond by the Fe^{IV}–oxo species to generate an Fe^{III}–hydroxide complex and a substrate radical; 7) rebound of a hydroxyl radical by the "oxygen rebound" mechanism[9] to afford the hydroxylated product and an Fe^{II} center; and 8) dissociation of the product.

The steps that precede the addition of oxygen to the Fe^{II} center have been studied in detail by Solomon and co-workers for several αKG-dependent hydroxylases and halogenases by means of circular dichroism and magnetic circular dichroism spectroscopy.[10] The hallmark features are bidentate binding of αKG to the Fe^{II} center, which gives rise to a metal-to-ligand charge transfer (Fe^{II} to α-ketoacid) band, and dissociation of the remaining water ligand upon substrate binding, which results in the creation of an open coordination site for oxygen to bind. These conclusions are corroborated by X-ray crystallographic studies.[11]

Application of a combination of rapid kinetic and spectroscopic techniques to the reaction of TauD resulted in the detection of two intermediates. Mössbauer and EPR spectroscopy suggested that the first intermediate is best formulated as a high-valent Fe^{IV} species (termed **J**) with an unusual HS (S=2) configuration.[12] Use of the 1,1-[D_2]taurine isotopomer results in a large deuterium kinetic isotope effect (^{2}H-KIE) of around 50 on the decay of **J**, which demonstrates that this intermediate is responsible for hydrogen-atom abstraction.[13] In the consensus mechanism, the C–H-cleaving species is proposed to be the Fe^{IV}–oxo (ferryl) complex (III). The presence of the ferryl unit was experimentally verified by resonance Raman spectroscopy, which exhibited an Fe–oxo stretching mode at 821 cm^{-1} that was downshifted to 787 cm^{-1} upon use of $^{18}O_2$,[14] and by X-ray absorption spectroscopy, which demonstrated that **J** has a very short iron–ligand interaction (1.62 Å) that is typical for the Fe^{IV}–oxo group.[15] Considerable insight into the geometric and electronic structure of this key reaction intermediate was obtained by comparing experimentally observed spectroscopic parameters to those calculated by density functional theory (DFT) for various hypothetical model structures of **J**, which suggest that **J** has either a trigonal bipyramidal or a distorted octahedral geometry.[16] Ferryl reaction intermediates with similar spectroscopic properties have been experimentally observed in several other mononuclear Fe^{II}-dependent

enzymes.[17] The second intermediate that accumulates upon reaction of the enzyme/Fe^{II}/αKG/substrate complex with oxygen is an Fe^{II} product(s) complex.[17a,c,e,18]

Insight into the oxygen activation at an α-ketoacid-ligated Fe^{II} center was also obtained from low-molecular-weight inorganic complexes.[19] The structures of the model complexes show that the α-ketoacid can bind to the Fe^{II} center in a mon odentate or a bidentate mode.[20] Comparison of the diagnostic metal-to-ligand charge-transfer transition of the enzyme/Fe^{II}/αKG complexes to those of the model complexes indicates that αKG must be bound to the metal in a bidentate way at the enzyme active site. The acceleration of decarboxylation caused by electron-withdrawing substituents on the α-ketoacid in the model complexes is in line with the proposed nucleophilic attack of the distal O atom derived from the oxygen on C2 of the α-ketoacid.[19b] Que and co-workers reported an excellent functional model compound for the αKG-dependent dioxygenases, [Fe(Tp^{Ph2})(BF)] (Tp^{Ph2}=hydrotris(3,5-diphenylpyrazol-1-yl)borate, BF=benzoylformate).[19a,b] Upon reaction with O_2, this complex is able to hydroxylate one of the phenyl rings of the Tp^{Ph2} ligand coupled with decarboxylation of the BF ligand, as confirmed by isotope labeling experiments; this reaction captures several of the salient features of the Fe^{II}- and αKG-dependent enzymes, that is, decarboxylation of the coordinated α-ketoacid and generation of the ferryl intermediate. However, the reactivity of the ferryl intermediate presumably entails an electrophilic attack on the electron-rich benzene ring, as was observed for the recently discovered Fe^{II}- and αKG-dependent epoxidase DdaD,[21] the enzyme 4-hydroxyphenyl-pyruvate dioxygenases (HPPD),[22] and the related Fe^{II}- and tetrahydropterin-dependent aromatic amino acid hydroxylases.[23] Recently, the proposed Fe^{IV}–oxo intermediate formed by oxygenation of the above complex was found to oxidize hydrocarbons with some shape selectivity.[19c] Moreover, several Fe^{IV}–oxo complexes, analogues of **J**, have been synthesized and characterized by various spectroscopic techniques (for a recent review, see ref. [24]). Although most of those complexes have an intermediate-spin (*S*=1) ground state, more recently, several examples of high-spin ferryl model complexes have been reported.[25]

DFT studies on oxygen activation in αKG-dependent enzymes and related model complexes have been performed,[26] but a consensus mechanism has not yet emerged from these studies. The DFT results suggested that in the enzyme system the reaction of oxygen activation takes place on the quintet surface.[26a] Specifically, the distal O atom of **I** performs a nucleophilic attack on the carbonyl group in αKG through a bicyclic transition state (TS) similar to the proposed intermediate **II** to afford a Fe^{II}–peroxosuccinate complex and CO_2; further heterolytic cleavage of the O–O bond in the peroxosuccinate yields an Fe^{IV}–oxo species, in which the formation of the Fe^{II}–peroxosuccinate complex was found to be the rate-determining step.[26a,b] In a different report, the same reaction was also suggested to proceed on the quintet surface.[26d] However, the proposed bicyclic structure **II** was identified as a local minimum derived from the nucleophilic attack of intermediate **I** on the carbonyl carbon in αKG. Following this step, release of CO_2 generated the same Fe^{II}–peroxosuccinate complex, whereas cleavage of the peroxo O–O bond to yield an Fe^{IV}–oxo intermediate was shown to be the rate-limiting step.[26d] Recently, Solomon and co-workers proposed that the enzymatic reaction might start from the triplet O_2 adduct, and that the rate-determining step is the triplet–quintet spin-crossover of the bi cyclic intermediate **II**.[26e] In the case of the biomimetic model complex [Fe(Tp^{Ph2})(BF)], DFT calculations showed that the oxygen activation process proceeds along a concerted reaction pathway on the septet surface in which the O–O bond in O_2 and the C1–$_{C2}$ bond in αKG are simultaneously cleaved.[26c]

Despite this considerable body of work, there are still a number of open questions. Why is the cosubstrate αKG indispensable to the reactivity of this family of nonheme iron enzymes? What is the difference of the reaction mechanism on the quintet and septet surfaces? In the

present work, we attempt to address these questions through detailed electronic-structure calculations of the catalytic cycle in the three alternative spin states. The cosubstrate αKG has a dual role, namely, it acts not only as an electron acceptor to stabilize the superoxide monoanion (the one-electron-reduced form of the cosubstrate O_2) to facilitate the second electron transfer, but also as an electron donor to provide the second and third electrons for the further reduction of the superoxide. One prominent feature of the present work is the use of single and multireference-correlated ab initio methods in addition to DFT. Thus, the energies of the local minima and saddle points on the potential-energy surface (PES) were calculated with the highly correlated ab initio coupled cluster singles and doubles with perturbative triples [CCSD(T)] method in an attempt to proceed beyond the accuracy and reliability inherent to standard DFT methods. In addition, the strongly contracted second-order *n*-electron valence space perturbation theory (NEVPT2)[27] was used on top of complete active space self-consistent field (CASSCF) wavefunctions to shed light on the intricate details of O_2 binding to a HS Fe^{II} center.

Results and Discussion

Energetics

The overall energy profile of the catalytic cycle—Reaction of the five-coordinated HS ferrous center (S_{Fe}=2) with triplet oxygen (S_{O_2}=1) led to three possible total spin multiplicities: septet (*S*=3), quintet (*S*=2), and triplet (*S*=1). Recently, a singlet O_2 adduct was suggested to be implicated in the oxygen-activation process of cysteine dioxygenase (CDO).[28] However, the singlet O_2 adduct of the TauD system was calculated to be approximately 14 kcal mol^{-1} higher in energy than the corresponding triplet species, and thus has not been investigated further. Figure 1 shows the PES of the three spin states for the oxygen activation by TauD calculated by the B3LYP density functional in the present work. Clearly, there are large differences in the number and energies of the intermediates and transition states along each reaction pathway (Table 1). A comparison to previous results in the literature will be provided after discussing the most salient features of the calculated PES.

Oxygen binding—If one considers the adiabatic approach of a triplet O_2 molecule to a quintet ferrous center, there are three spin states that can arise: triplet, quintet, and septet. Furthermore, since distorted octahedral ferrous centers are orbitally near-degenerate (the ground state derives from a low-symmetry split $^5T_{2g}$ term), there are up to nine electronic states that may be low-lying enough to warrant further analysis. In DFT calculations one can only (and even here only approximately) access three of these states, namely, the lowest energy triplet, quintet, and septet states. In the present case, the low-symmetry effects are large enough to leave a single-orbital configuration at the iron center lowest in energy and hence it is sufficient to concentrate on the three lowest-energy electronic states with triplet, quintet, and septet spin multiplicities.

According to the B3LYP results, the three spin states are very close in energy with the order triplet < septet < quintet. However, one should note that the energy differences of less than 2 kcal mol^{-1} are within the uncertainty of the methodology. Consistent with previous studies,[26] the binding of O_2 to the iron center is calculated to be endergonic on all three investigated PES. Taken at face value, this may suggest that theory predicts that the chemistry observed for the Fe^{II}- and αKG-dependent enzymes cannot happen. However, Friesner and co-workers have shown that there is a large protein contribution to the free energies of oxygen addition reactions that can make the reactions more exergonic by as much as 10 kcal mol^{-1}.[29] Thus, the actual situation in the protein is more favorable, and the oxygen-binding step may be even slightly exergonic as observed in hemerythrin[30] and model systems.[31]

An important aspect of the calculations is that, following oxygen binding to the Fe^{II} center, the three spin states barely split (less than 2 kcalmol ^{1}). This result has not been anticipated as normal reactions between open-shell fragments will tend to lead to repulsive surfaces for ferromagnetic spin alignment and deep wells that correspond to bond formation for antiferromagnetic spin alignment. To obtain more insight into the O_2 addition step, we have resorted to multiconfigurational ab initio quantum chemistry, which has the advantage that on all PES, the many particle wavefunctions can be properly represented by spin eigenfunctions. As described in the Experimental Section, CASSCF calculations with a large 16-in-13 active space were carried out on the small model to study the oxygen-binding process. Dynamic correlation effects were covered with the NEVPT2 method.

Consistent with the B3LYP results, CASSCF and NEVPT2 calculations show that the triplet, quintet, and septet O_2 adducts are energetically within 4 kcal mol^{-1} of each other (Table 2). Equally consistently, all multiconfigurational calculations predict the triplet species to be lowest in energy. By using the CASSCF and NEVPT2 methods, the quintet and septet species are estimated to be almost degenerate with the quintet complex being lower in energy. The differences between the septet and quintet O_2 adducts only amount to a few tenths of 1 kcal mol^{-1}. Both results are consistent with CCSD(T) calculations, which deliver slightly larger energy separations between the different spin multiplicities. However, even here the septet species is predicted to be only 6.3 kcal mol^{-1} higher than the triplet analogue. It thus appears to be safe to conclude that for the O_2 adduct of TauD there are three low-lying states of different spin multiplicities, all of which could serve as the basis for further reactivity.

The calculated PES for O_2 binding by using CASSCF and NEVPT2 methods on structures obtained from relaxed surface scans are shown in Figure 2. In contrast to the B3LYP results that estimated O_2 addition to be marginally endothermic ($\approx$3 kcal mol^{-1}), the CASSCF and NEVPT2 calculations show that the oxygen-binding process is moderately exothermic by approximate 10 kcal mol^{-1}. Thus, the binding energy may cancel out the entropy term ($\approx$10 kcal mol^{-1}) for oxygen addition and hence leads to the binding process being nearly thermoneutral. In nonheme iron proteins, both factors (the environmental effects and the moderate exothermic addition of O_2) may make the O_2 addition take place easily as observed experimentally.[30,31] As expected, all three spin states are nearly degenerate at $Fe–O_2$ distances beyond 2.4 on account of the lack of interaction between the ferrous active site and O_2. At shorter distances, the formation of a weak bond preferentially stabilizes the triplet O_2 adduct. However, in the entire process of O_2 binding, the quintet and the septet complexes remain nearly degenerate with the quintet species lying at marginally lower energy. The dynamic correlation energy brought in by the NEVPT2 correction does not appreciably change the situation.

The first transition state—The most straightforward situation exists on the septet surface. Following binding of O_2, the system passes through a single TS, the bicyclic peroxyhemiketal complex, to afford an oxo-like species with concomitant decarboxylation of the αKG cosubstrate. It will be shown below that on this surface, the bonding of this intermediate is best described as a HS ferric ion bound to an oxyl radical. Thus, on the septet surface, decarboxylation of αKG appears to be concurrent with the cleavage of the O–O bond to form a Fe^{III}–oxyl compound.

On the quintet surface, a much more complicated stepwise reaction mechanism is operative. Following oxygen addition, the quintet O_2 adduct traverses through a decarboxylation TS that is geometrically and electronically similar to that found on the septet surface and then releases CO_2 to yield an Fe^{II}–peroxosuccinate complex that is accompanied by a large drop in energy. Subsequently the O–O bond is broken by means of two single-electron transfer

steps via the half-bond intermediate (see Figure 1) to produce the experimentally observed quintet Fe^{IV}–oxo intermediate that functions as a C–H cleaving agent.

Finally, on the triplet surface the first TS is difficult to locate. However, we noted that the energy of the triplet bicyclic intermediate **II** is already approximately 5 kcal mol^{-1} higher than ^{5,7}TS1 on the quintet and septet surfaces. It follows that an even higher barrier is needed to form this species; thus, the triplet surface can be ruled out as an explanation of the TauD dioxygen chemistry.

The energy profile displayed in Figure 1 is in good agreement with that reported by Siegbahn et al. in ref. [26a] except for the relative free energies for ^{5}TS1 and ^{7}TS1. As indicated by their electronic structures (vide infra), these two species should be nearly isoenergetic; according to our results described below, it is the difference in entropy that leads to the slightly lower free energy of ^{7}TS1.

Calculations of PES with the small model by using B3LYP and CCSD(T) methods were performed. Overall, the B3LYP PES of the small model are consistent with those of the large one with comparable barriers for the quintet and septet reaction channels (Table 3). However, in the case of ^{7}TS1, the barrier height predicted by the CCSD(T) calculations is approximately 4 kcal mol^{-1} lower than that estimated by B3LYP. Thus, for the real model, the B3LYP calculations may also slightly overestimate the barriers of the rate-determining steps. The significant difference occurs for the relative energies of the septet and quintet Fe^{IV}–oxo intermediates. It turns out that the energy difference between these two species is significantly underestimated by the B3LYP method. For the quintet ferryl species, the unrestricted Hartree–Fock (UHF) calculation converged to an electronic state that is best characterized as a HS ferric ion ($S_{Fe}=\frac{5}{2}$) bound to an oxyl radical (S_O=½) in an antiferromagnetic fashion. Consequently, the subsequent CCSD(T) calculations based on the UHF reference orbitals converged to the same erroneous electronic state (for further discussion, see ref. [32]). The calculations predict a marginal energy separation (3.5 kcal mol^{-1}) between the septet and quintet Fe^{IV}–oxo intermediates since both species have a nearly identical electronic structure except for the different spin coupling between the HS ferric center and the oxyl radical. To guide the CCSD(T) calculations to the correct electronic states that are in accordance with experimental data, orbitals from the CASSCF (CAS(10,8)) reference wavefunction had to be employed. Because coupled-cluster theory is known to be nearly invariant with respect to the choice of the reference determinant, such a choice is justified. Finally, the CCSD(T) calculations yielded an energy splitting of 26.1 kcal mol^{-1}. Moreover, the relative energies of the septet and quintet ferryl species were also computed by the simplified multireference spectroscopy-oriented configuration interaction (SORCI) method. The SORCI calculations on top of the CASSCF reference space (CAS(10,8)) estimated that the quintet species is stabilized by 23.7 kcal mol^{-1} in energy relative to the septet analogue. Both values are in good agreement with that delivered by the CASPT2 calculations on the Fe^{IV}–oxo intermediate of the αKG-dependent halogenases (27.2 kcal mol^{-1}).[33]

Electronic-structure analysis

In this section, insights into the calculated reaction pathway were obtained by means of a detailed analysis of the changes in the electronic structure that occur while traversing the various intermediates and TSs.

The O_2-bound species $\{FeO_2\}^8$—According to the energy profile of the oxygen activation, the O_2 adduct is the only candidate other than the ferryl species that may be trapped experimentally. Figure 3a exhibits the geometries of the O_2 adducts on the septet, quintet, and triplet surfaces. Table 4 summarizes key geometric parameters for them.

Comparison of the three geometries reveals that the most noticeable difference is the relative orientation of the O_2 moiety relative to αKG. In the septet and quintet O_2 adducts, the O_2 group is situated above the carbonyl group of αKG, whereas in the triplet species the O_2 motif is situated above the acetic acid of Asp. Recently, the $\{FeO_2\}^8$ adduct of the extra-diol dioxygenase was trapped and spectroscopically characterized.[34] It contains a HS ferric center ($S_{Fe}=\frac{5}{2}$) that is antiferromagnetically coupled to a superoxo π radical (S_{O_2}=½), thus yielding an overall quintet ground state (S=2).[34] The same electronic structure is found for the quintet O_2-bound species investigated here (Figure S2 in the Supporting Information). However, the corresponding O_2 adducts of the αKG-dependent nonheme iron enzymes have not been trapped and characterized; thus, the corresponding NO adducts, which are $\{FeNO\}^7$ complexes, have been prepared for many of these enzymes and served as a structural model for the $\{FeO_2\}^8$ state. Specifically, the $\{FeNO\}^7$ complex of the αKG-dependent enzyme clavaminate synthase (CS) has been structurally characterized in which the NO-derived O atom is situated above the αKG group.[35] Moreover, the iso-electronic $\{FeNO\}^8$ complex in TauD was generated by cryogenic reduction and characterized by Mössbauer spectroscopy.[36] The combined experimental and theoretical spectroscopic studies demonstrated that the TauD–$\{FeNO\}^8$ species is best described as having a triplet ground state that arises from antiferromagnetic coupling between a HS ferrous center (S_{Fe}=2) and a triplet NO^- (S_{NO}=1). This electronic-structure description is identical to what we found for the triplet O_2 adduct (vide infra), except that NO is replaced by O_2. In line with this observation, the proposed geometry of the triplet TauD–$\{FeNO\}^8$ species shows that the relative NO orientation with respect to αKG is similar to that of O_2 in the triplet O_2 adduct. Experimentally, septet O_2 adducts have not been detected thus far; according to our calculations, its electronic structure may best be rationalized as two resonance structures: 1) a HS Fe^{II} center (S_{Fe}=2) ferromagnetically coupled to a triplet O_2 (S_{O_2}=1), and 2) a HS Fe^{III} ion ($S_{Fe}=\frac{5}{2}$) bound to an $O_2^{-\cdot}$ radical ligand with S_{O2}=½ in a ferromagnetic fashion (Figure S1 in the Supporting Information). The detailed analysis of the geometric and electronic structures for O_2 adduct can be found in the Supporting Information.

The septet reaction mechanism—To understand the different reaction mechanisms of the oxygen activation on the alternative PES, the electronic structures of the key local minima will be separately discussed.

A salient feature of the septet reaction mechanism is that only a single TS is required to achieve the O_2 activation following O_2 binding. The optimized structures of the decarboxylation TS on the quintet and septet surfaces (^{5,7}TS1) are shown in Figure 3b. It is worth emphasizing at this point that in both cases the TSs have the bicyclic structure that is proposed to be an intermediate in the consensus mechanism (Figure 1). By contrast, according to our calculations, such bicyclic geometries do not exist as local minima on the quintet and septet surfaces but only as TS. However, a similar bi- cyclic intermediate has been detected in a single crystal of the extradiol catechole dioxygenases.[37]

The geometry of ^{7}TS1 exhibits a shorter O(O_2)–C2 and a longer C2–O(C=O) bond relative to those in the O_2-bound species, and the most noticeable geometric feature is the significantly elongated C1–C2 bond (2.5 Å) in αKG (Table 5). This indicates that the C2=O double bond of the carbonyl group has changed to a single bond. This process is accompanied by formation of a single bond between the C2 atom of αKG and the distal O atom of O_2 and by partial cleavage of the αKG $C1-_{C2}$ σ bond.

A qualitative molecular orbital (MO) scheme of ^{7}TS1 is depicted in Figure 4a. In the upper valence region, the five unpaired electrons reside in the five Fe 3d-based MOs; the last singly occupied MO represents the αKG $C1-_{C2}$ σ-bonding orbital. Thus, the electronic structure of ^{7}TS1 is best formulated as a HS ferric ion ($S_{Fe}=\frac{5}{2}$) ferromagnetically coupled to

a C–C σ radical (S_{CC}=½). By inspection of the localized MOs on the O_2 moiety, one can identify that the O–O σ-bonding MO and two atomic p orbitals on each O atom are doubly occupied. This implies that there is no net π-bonding interaction left in the O_2 fragment, but that the O–O σ bond is still intact. Thus, the O_2 moiety is best interpreted as a peroxy-level species, and at that stage of the reaction cycle the two-electron reduction of O_2 has been accomplished. It follows that, relative to the O_2 adduct, one electron has been transferred from the HS ferrous center to O_2, and the other electron originates from the C1–C2 σ-bonding orbital. In ^{7}TS1, a σ bond between the distal O atom of O_2 and the αKG C2 atom is formed, similar to intermediate **II** in the proposed mechanism. However, intermediate **II** does not exist as an intermediate on either the quintet or the septet surface, but rather represents a TS.

To gain further insight of the electronic structure changes into the mechanism by which the system approaches ^{7}TS1, an MO diagram of a pre-^{7}TS structure is presented in Figure 5a. It was obtained by fixing the C1–C2 distance to 1.80 Å in the relaxed surface scan. The electronic structure of this pre-TS1 may be best rationalized as a HS ferric center ($S_{\mathrm{Fe}}=\frac{5}{2}$) ferromagnetically coupled to a four-center radical with the spin being delocalized over the O-O-C1-C2 fragment. The four-centered radical SOMO is composed of the O_2 π_{op}* and the αKG C1–C2 σ-fragment orbitals. Thus, one can deduce that for the oxygen activation the first electron comes from the HS ferrous center and the O_2 π_{ip}* orbital acts as the first electron acceptor. The second electron transfer between the O_2 π_{op}* and the C1–C2 σ MO appears on the way to ^{7}TS1 at the present stage.

The decay of ^{7}TS1 was also investigated by a relaxed surface scan in which the O–O bond was successively lengthened. The MO diagram of a species with an O–O bond length of 1.70 Å is displayed in Figure 5b. This species contains a HS ferric ion ($S_{\mathrm{Fe}}=\frac{5}{2}$) that is ferromagnetically coupled to an O–O σ* radical (S_{O_2}=½). Thus, after traversing ^{7}TS1, the electron that previously occupied the C1–C2 σ orbital shifts into the O–O σ* orbital to perform the third electron reduction of O_2. At this point the final O–O σ bond tends to break. Eventually, the O–O bond cleavage leads to an Fe^{III}–oxyl species as the final product of oxygen activation on the septet surface (Figure S4 in the Supporting Information). This assignment is corroborated by the calculated isomer shift of 0.57 mm s^{-1}, which is typical of HS Fe^{III}.[38]

Relative to the quintet ground state of the Fe^{IV}–oxo species (vide infra), the septet $(FeO)^{2+}$ core is approximately 16 kcal mol^{-1} higher in energy[39] and may be interpreted as a ligand-to-metal charge transfer (LMCT) spin-flip excited state. It should easily decay into the quintet counterpart by “de-excitation” of the electron in the σ-antibonding Fe d_{z2} MO into the π-bonding O p_x orbital concomitant with a spin flip that may be transmitted by an efficient spin–orbit coupling pathway and large driving force.

Quintet reaction mechanism—On the quintet surface, the first electron transfer takes place upon addition of O_2 to the HS ferrous center, thus leading to a HS ferric ion antiferromagnetically coupled to a superoxo radical in the O_2 adduct (vide supra).

As depicted in Figure 4b, a decarboxylation TS (^{5}TS1) similar to that found on the septet surface was located on the quintet surface. Compared to ^{7}TS1, the most remarkable difference is the much shorter C1–C2 bond length in ^{5}TS1 (2.5 Å in ^{7}TS1 versus 1.7 Å in ^{5}TS1), thereby reflecting that ^{5}TS1 is a relatively “early” TS for the decarboxylation of αKG. The electronic structure of ^{5}TS1 closely resembles that of ^{7}TS1 except that an electron with opposite spin to the majority iron spin resides in the C1–C2 σ-bonding orbital. Thus, the bonding situation is best rationalized as antiferromagnetic coupling between a HS Fe^{III} ($S_{\mathrm{Fe}}=\frac{5}{2}$) and a C–C σ radical ($S\propto$=½). Analogous to ^{7}TS1, the O_2 motif is in a peroxy-level

state. Given the relatively large distance between these two exchange-coupled fragments, the electronic energy of ^{5}TS1 should be nearly identical to that of ^{7}TS1. In fact, B3LYP predicts that ^{5}TS1 lies 0.5 kcal mol^{-1} lower in energy than the corresponding ^{7}TS1. However, if one regards the release of CO_2 as a decomposition reaction, the entropy effect should favor ^{7}TS1 since the septet decarboxylation reaction proceeds more completely, as evidenced by the much longer C1–C2 distance. As a consequence, ^{5}TS1 lies 2.1 kcal mol^{-1} higher in the free energy than the corresponding ^{7}TS1. However, since the entropic contributions to the TS are only crudely modeled in these calculations, the energetic ordering of the septet and quintet TS is certainly open to debate.

The fact that in ^{5}TS1 the σ-radical electron is aligned anti-parallel to the iron spin has decisive consequences for the further reactivity. After passing through ^{5}TS1, the β electron in the C1–C2 σ orbital shifts to the HS Fe^{III} center instead of the O–O σ bond, thus forming a HS Fe^{II} center (S_{Fe}=2) bound to a peroxosuccinate (Figure S5 in the Supporting Information). This electronic-structure description is corroborated by the calculated isomer shift of 0.99 mms^{-1}, which is typical of HS Fe^{II}. However, the same electron-transfer pathway is spin-forbidden on the septet surface because an a electron rather than a β electron resides in the C1–C2 σ orbital in the corresponding TS (^{7}TS1). Therefore, the α electron can only move into the low-lying unoccupied O–O σ* orbital during the decay of ^{7}TS1.

To accomplish the four-electron reduction of O_2, two electrons (one α and one β) are still required to be shifted into the O–O σ* orbital so as to completely cleave the O–O bond. On the quintet surface, we found that the two-electron transfer needs two steps before ending up with the experimentally characterized Fe^{IV}–oxo species: a β-electron transfer from the Fe d_{xy} orbital to yield a "half-bond intermediate" followed by an α-electron transfer from the Fe $d_{z2/xz}$ orbital. (The MO diagrams of the relevant local minima and saddle points are gleaned in the Supporting Information.) The TS that connect the relevant minima are extremely low in energy such that these two electron-transfer reactions should occur very fast and the intermediates do not accumulate to levels that allow for their spectroscopic characterization.

Triplet reaction mechanism—In the case of the oxygen activation on the septet and quintet surfaces, the first electron-transfer pathway involves the HS ferrous center and the O_2 π_{ip}* orbital. If the same electron-transfer process took place from the triplet O_2 adduct (best formulated as HS Fe^{II} anti-ferromagnetically coupled to $^3O_2$), one would obtain an intermediate spin (IS) Fe^{III} ($S_{Fe}=\frac{3}{2}$) coupled to a superoxo radical (S_{O_2}=½) in an antiferromagnetic fashion. However, the IS Fe^{III} ion cannot be stabilized by the weak field ligands provided by the TauD active site. It follows that this electron-transfer step would be accompanied largely by a structural rearrangement of the entire first coordination sphere of the iron center. Hence, a very high energy barrier is expected. Unfortunately, we have not been able to successfully locate the relevant TS. Instead, the proposed bicyclic intermediate **II** was found to be a real intermediate on the triplet surface, rather than a TS as calculated on the septet and quintet surfaces. However, it turns out that the bicyclic intermediate is destabilized by 4.6 kcal mol^{-1} in energy relative to ^{7}TS1. This observation rules out the possibility that the O_2 activation can proceed on the triplet surface. Therefore this surface was no longer investigated.

On the role of αKG—For the septet mechanism, there essentially occurs a two-electron-transfer step from the O_2 adduct to achieve the decarboxylation of αKG in ^{7}TS1. Due to the fact that the electron affinity of the superoxide anion is substantially lower than that of neutral dioxygen, the direct reduction of superoxide to a peroxo-level product should be energetically very costly. Thus one might argue that another intermediate might exist before approaching ^{7}TS1. However, this does not appear to be the case. It signifies that there are subtle electronic effects that compensate for the attenuated electron affinity of the O_2 group

following one-electron reduction and therefore allow for the second electron transfer to happen. In analogy to the quintet reaction channel, the first electron transfer on the septet surface is achieved by transferring an electron from the HS ferrous center to the O_2 π_{ip}* orbital, which should produce a HS ferric ion ($S_{Fe}=\frac{5}{2}$) that is ferromagnetically coupled to a superoxo radical (S_{O_2}=½). In fact, a similar electronic structure was found for the quintet O_2-bound species, except that these two fragments are antiferromagnetically coupled. The nucleophilic attack of superoxide on carbonyl group in αKG results in the electron transfer from the doubly occupied O_2 π_{ip}* orbital into the αKG LUMO, which is mainly the C=O π* orbital and eventually transforms the αKG carbonyl group into an alkoxide.[26e] As a consequence, the negative charge is effectively transferred from the superoxide to αKG, and accordingly the electron affinity of the O_2 fragment is restored. On the other hand, the nucleophilic attack can be viewed as a two-electron reduction of αKG. This should lower the oxidation potential of αKG and render it easily oxidizable. Therefore, the second electron transfer from the αKG HOMO, which is largely composed of the C1–C2 σ orbital, can easily occur, thereby leading to a C–C σ radical.

Due to the fact that α-keto acids are stable in air, the above discussion raises the question of why such nucleophilic attack only occurs in the enzyme. As described above, the αKG LUMO functions as a two-electron acceptor. The energy of the electron accepting orbital obviously affects the efficiency of the electron transfer. As noted previously, the binding of αKG to the Fe center dramatically lowers the energy of the αKG LUMO.[10a] Because the C1–C2 bond in αKG is a single bond, the carbonyl and carboxylate groups are not coplanar in the free αKG. However, once it coordinates to the Fe center as a bidendate ligand, the two groups are forced to be coplanar so that the π-conjugation system is enlarged. Thus the bidentate bonding mode of αKG in the active site of the enzyme stabilizes its LUMO and enhances the capability of its LUMO to serve as an electron acceptor (Figure 6). On the other hand, the contribution from the C=O π* orbital to the αKG LUMO is reduced due to the extended π-conjugation. One may argue that the overlap between the O_2 π_{ip}* orbitals and the C=O π* orbitals would be diminished, which would disfavor bond formation between them. However, the relative contribution of the carbon p orbital to the C=O π* orbital increases because the binding of the carbonyl group to the Fe center brings down the energy of the oxygen-derived atomic p orbitals. The second effect will overcompensate the first one and increase the nucleophilicity of αKG (electrophilic assistance).[8] In the active site of the enzyme, the αKG LUMO has a much lower energy and a larger contribution of C p orbitals. Both factors work in synergy to make the enzyme work in the way it does.

Comparison of the computationally predicted reaction pathway to experimental data—Using the calculated reaction energies and free-energy barriers for oxygen activation (see Table 1) as well as those for hydrogen-atom abstraction taken from ref. [39b], the Arrhenius equation was set up for each step of the reaction. Assuming the forward and backward reaction of each step was in equilibrium, we computed the relative amounts of key intermediates of the catalytic cycle at each time point by numerically solving the simultaneous rate equations.

As shown in Figure 7, the ferryl species is the only intermediate that, according to our calculations, is expected to accumulate to significant levels during the reaction. Perhaps the most significant uncertainty for this analysis is the predicted accumulation of the $\{FeO_2\}^8$ adduct to very low levels, because the large protein contribution to O_2 binding renders its relative energy uncertain.[29] However, the fleeting nature of the $\{FeO_2\}^8$ intermediate is also borne out from experiment. First, we have calculated the Mössbauer parameters of the $\{FeO_2\}^8$ complexes (see Supporting Information). For the quintet and septet $\{FeO_2\}^8$ complexes, this analysis predicts that their high-energy lines are at 1.04 and 1.29 mms ^{1}, respectively, that is, it would not overlap with the ferryl intermediate or the Fe^{II}-containing

reactant or product complexes. From the freeze-quench (FQ) Mössbauer spectra reported previously,[12a,18] we can effectively rule out accumulation of such a species to more than 5% of the total Fe. The triplet $\{FeO_2\}^8$ complex is best described as a HS Fe^{II} complex. Its high-energy line is predicted to be at 2.45 mms ^{1} and would therefore overlap significantly with the features of the Fe^{II}-containing reactant and product complexes and not allow for its unambiguous detection. Second, the approximate first-order dependence of the absorption features of the ferryl intermediate on $[O_2]$ reveals that if an intermediate state that preceded the ferryl intermediate were to accumulate rapidly, it would accumulate to around 0.3 equiv after approximately 1 ms of reaction time.[18] Taken together, the experimental kinetic and spectroscopic data is consistent with our prediction that the $\{FeO_2\}^8$ complex does not accumulate. Likewise, additional intermediates past the first transition state on the quintet surface also do not accumulate to levels detected by spectroscopic methods because the barriers for their interconversions are so low that the reactions will be extremely fast.

Discussion

In this paper, we have given a detailed interpretation of the electronic-structure changes occurring during oxygen activation in the active site of Fe^{II}- and αKG-dependent nonheme enzymes. To this end, we have investigated the three feasible PES with triplet, quintet, and septet spin multiplicities, respectively. In terms of the calculated structures and energies our results are, apart from some small details, consistent with the earlier work by Siegbahn,[26a] but deviate in some aspects from the analogous studies reported by de Visser and Solomon.[26d,e] Notably, a different density functional (BP86) was employed in the study reported in ref. [26e]. In our previous work,[36] the B3LYP functional has been used to evaluate the electronic structure of the TauD–$\{FeNO\}^7$ and TauD–$\{FeNO\}^8$ species with the latter being isoelectronic with the O_2 adduct. The calculated spectroscopic parameters based on the predicted electronic structure successfully reproduce the experimental data, thereby lending credence to the employed computational method in the present work. The reasons for the discrepancies with the study reported in ref. [26d] that was also carried out with the B3LYP functional are not clear. Our calculations revealed that the nucleophilic attack of the distal O atom of the O_2 adduct on the carbonyl group in αKG via a bicyclic transition state (TS1) is the rate-limiting step, which is between the addition of O_2 to the enzyme:Fe^{II}/αKG/substrate complex and the generation of the Fe^{IV}–oxo intermediate, as confirmed by recent experimental studies.[40] Decay of ^{7}TS1 affords a HS Fe^{III} bound to an oxyl radical, whereas ^{5}TS1 evolves into a HS Fe^{II} chelated by peroxosuccinate. According to the calculated energetics using DFT and ab initio methods, the septet reaction pathway might compete with the quintet channel.[41] This might help to reconcile the discrepancies in the reaction pathways between the model complex [Fe(Tp^{Ph2})(BF)] and the enzyme. In the former, O_2 activation is proposed to proceed on the septet surface, whereas the quintet mechanism is suggested to be the reaction channel for the latter. A qualitative difference was found in a different study in which the quintet bicyclic structure **II** was identified as a local minimum rather than a TS, and the cleavage of the peroxo O–O bond is suggested to be the rate-determining step.[26d]

The new aspect of this work is the detailed electronic-structure interpretation and, secondly, the use of highly correlated ab initio methods for the investigation of the reaction mechanism. We will highlight these chemical and methodological advances below. Quite surprisingly, the interaction of the five-coordinate quintet Fe^{II} active site in αKG-dependent nonheme iron enzymes and $^3O_2$ does not lead—as in normal radical reactions—to a substantial splitting of the possible PES. Rather, the quintet, and septet states of the system remain essentially degenerate throughout the approach of O_2 to the active site with the triplet species lying slightly lower in energy (<4 kcal mol^{-1}). However, following the thermoneutral O_2 binding step, only the quintet and septet reactions are kinetically feasible

whereas the triplet surface is energetically inaccessible. This is readily traced back to the fact that the first electron transfer from the HS Fe^{II} ion to O_2 on the triplet surface would lead to an IS Fe^{III} center that cannot be stabilized by the ligand framework in nonheme iron proteins.

On the septet and quintet surface, analogous TS are found in which two electrons have been transferred to the O_2 fragment: one electron derives from the iron center and the other from the αKG cosubstrate. The geometries of ^{5,7}TS1 closely resemble the proposed bicyclic intermediate **II**. However, on neither surface does a genuine bicyclic structure exist as an intermediate; instead this structure represents a TS. This is a major change relative to the formulated consensus mechanism that had been proposed more than 20 years ago.[8] The quintet and septet TS differ in their electronic structure mainly in the fact that on the septet surface, the αKG σ radical is coupled ferromagnetically to the HS Fe^{III} center, whereas on the quintet surface the coupling is antiferromagnetic. Since the two exchange-coupled fragments are well separated, the coupling is very weak and ^{7}TS1 and ^{5}TS1 are therefore nearly isoenergetic. The energetic near-degeneracy between ^{7}TS1 and ^{5}TS1 results from the similarity of their electronic structures; hence, one may anticipate that the influence that arises from the protein environment on their relative energetics should be quite limited.[33] However, the distinct spin coupling has major consequences on further reactivity. On the septet surface, the system is forced to execute the next electron transfer into the O–O σ* orbital, thus leading to immediate cleavage of the O–O bond and formation of the Fe^{III}–oxyl intermediate. On the quintet surface, however, the unpaired electron from the αKG s radical can be transferred in a spin-allowed fashion directly to the iron center, thereby yielding a Fe^{II}–peroxosuccinate intermediate that then decays quickly to the Fe^{IV}-oxo species. To the best of our knowledge, this insight into the observed shapes of the three PES has not been put forward before.

In the present study, the role of the cosubstrate αKG is also discussed. Upon the initial formation of superoxide radical by electron transfer from the ferrous active site, the electron affinity of the O_2 fragment is significantly attenuated. Thus, the system requires an electron acceptor to recover the electron affinity of the O_2 moiety to facilitate the second electron-transfer step. This electron acceptor is the LUMO of αKG. The nucleophilic attack of the superoxide on the C=O group in αKG is essentially a two-electron transfer process from the O_2 π_{ip}* orbital into the αKG LUMO that is accompanied by formation of a σ bond between the distal O and C2 atoms. This bond may then serve as a conduit for the further electron transfer from αKG to the O_2 moiety. More importantly, during this process the αKG cosubstrate is reduced, which in turn facilitates the second electron transfer from its HOMO to the iron center.

Our DFT results have been backed up with results from high-level ab initio methods obtained for the small models of the active site. First of all, CASSCF and NEVPT2 calculations were used to investigate the qualitative behavior of the three spin states upon O_2 binding without the issue of spin contamination or broken symmetry. Overall, the results essentially confirm the picture delivered by the B3LYP functional, despite the fact that the B3LYP calculations may slightly overestimate the barrier height relative to the energies delivered by the high-level CCSD(T) method. An interesting case has been identified for the septet–quintet separation in the $(FeO)^{2+}$ species. Here, the quintet UHF reference wavefunction is qualitatively wrong and corresponds to a HS Fe^{III}–oxyl description rather than the correct Fe^{IV}–oxo formulation. Consequently, the CCSD equations converge to a qualitatively erroneous state that is high in energy. This can be remedied by feeding the natural orbitals of a reasonably sized CASSCF calculation—which does yield a qualitatively correct electronic structure—into the CCSD(T) procedure. In this way one obtains a much lower energy of the quintet species, and the computed septet–quintet separation is in good

agreement with the multireference SORCI calculations. Hence, this result serves as a significant warning that one has to very carefully investigate the reference determinant for coupled-cluster-type calculations on open-shell transition-metal complexes since in many cases it will be qualitatively wrong, and even the powerful coupled-cluster procedure cannot compensate for a qualitatively erroneous electronic configuration.

Conclusion

In the present contribution, a detailed analysis of the electronic structure changes that occur in the oxygen activation by Fe^{II}- and αKG-dependent nonheme enzymes was performed. The reaction may take place either on the septet or on the quintet surfaces with the same rate-limiting steps, whereas the triplet reaction channel is catalytically irrelevant. For the septet mechanism, only one step is required to achieve oxygen activation. By contrast, the quintet mechanism features a multistep pathway. High-level ab initio calculations have been used to verify DFT results and thus lend credence to our conclusions.

The biological role of the cosubstrate αKG is discussed. It functions not only as a two-electron donor, which has long been identified, but also, and in our opinion more importantly, as an electron acceptor.

Experimental Section

All calculations were performed with the ORCA program package.[42] Our models are based on the crystal structure of TauD (PDB code: 1 gqw).[11b] We employed an active-site model of TauD in which an iron center is coordinated by two imidazole ligands (His) and one acetate ligand (Asp) to form a facial plane, and one α-ketopropionate (αKG) that occupies the equatorial plane.

The hybrid B3LYP density functional[43] was used in combination with the triple-ζ quality TZVP[44] basis sets on Fe, O, and N, and the SV(P)[45] basis sets were used on the remaining atoms. The RIJDX[46] approximation was used to accelerate the calculations using the auxiliary basis sets TZV/J (Fe, O, and N) and SV/J (the rest).[47] The geometry optimizations were performed without constraints. The subsequent numerical frequency calculations verified that all structural local minima display real frequencies only and TS are characterized by a single imaginary frequency. The zero-point energies, thermal corrections, and entropy terms for the optimized geometries were obtained from the frequency calculations.

A previously introduced general notation BS(m,n)[48] was adopted to denote several broken symmetry solutions to the spin-unrestricted Kohn–Sham equations. The nature of these solutions was revealed by the corresponding orbital transformation,[49] which, by means of the corresponding orbital overlaps, demonstrates whether the system is to be described as a spin-coupled or an almost spin-pure solution.[48]

Final energy calculations were performed with the hybrid B3LYP density functional by using the def2-TZVPP basis sets that are of triple-ζ quality and include high angular momentum polarization functions for all elements. The density fitting and “chain of spheres” (RIJCOSX)[50] approximations were employed in these calculations. The effect of the RIJCOSX approximations on the relative energies reported here have been verified to be less than 1 kcal mol^{-1}, yet the calculations are up to 50 times faster.[50] The protein environment was crudely modeled by the conductor-like screening model (COSMO)[51] model. As suggested by Siegbahn,[52] the dielectric constant was taken to be 4.0.

A smaller model in which the His residues were replaced by NH_3, Asp by OH^-, and αKG by α-ketopropionate was employed to use computationally demanding wavefunction-based ab initio methods for the calculation of selected points on the PES. Namely, the CCSD(T) method was used to calculate the energy profiles of the quintet and septet states. In all ab initio calculations, the TZVP (Fe, O, N, and C) and SV(P) basis sets (hydrogen elements) were applied. Given the computational cost, the basis sets employed are reasonable although they are certainly not able to recover the entire correlation energy. The reliability of model truncation was checked with DFT calculations on the same model in comparison with the nontruncated model. It turns out that the results are generally very similar and have an energy difference less than 3 kcal mol^{-1}, hence the comparison between ab initio results on the small model and DFT results on the large model is justified.

CASSCF and NEVPT2 calculations were carried out to compute the relative energies of the O_2 adduct with different spin multiplicities. In the active space, sixteen electrons are distributed into the five Fe 3d orbitals, the six O_2 valence orbitals (σ, σ*, 2π, and 2π*) and the π-bonding and the corresponding antibonding orbitals of the C=O group in αKG (CAS-(16,13)). To investigate the energy splittings between different spin multiplicities in the course of O_2 binding, relaxed surface scans with a series of Fe–O_2 distances on the triplet, quintet, and septet surfaces were performed using the small model. The relaxed surface was computed with the B3LYP method. At each point of the curve, the binding energy was calculated by the CASSCF (CAS(16,13)) method. In the vicinity of the equilibrium geometry, NEVPT2 calculations were conducted to capture dynamic correlation effects. NEVPT2 is similar to the popular complete active-space second-order perturbation theory (CASPT2) but is not plagued by intruder state problems.

For the quintet Fe^{IV}–oxo species and the corresponding septet species, we have performed CASSCF and more rigorous multireference configuration interaction (MRCI) calculations in form of the spectroscopy-oriented configuration interaction (SORCI)[53] on top of the CASSCF reference space. In the CASSCF calculations, the active space that consisted of ten electrons in the five Fe 3d orbitals and the three oxo p orbitals (CAS(10,8)) was chosen. In the SORCI calculations, the thresholds T_{pre}, T_{nat}, and T_{sel} were set to 10^{-5}, 10^{-5}, and 10^{-6} Eh, respectively.

Supplementary Material

Refer to Web version on PubMed Central for supplementary material.

Acknowledgments

The authors gratefully acknowledge financial support of this work from DFG (DFG-NE 690/7-1 to S.Y., F.N., J.M.B., and C.K.), from NSF (CHE-724084 to F.N., J.M.B., and C.K., and MCB-642058 to J.M.B. and C.K.), from the special research unit SFB 813 Chemistry at Spin Centers (to S.Y., F.N.) and from NIH (GM-69657 to J.M.B. and C.K.).

References

1. Hausinger, RP.; Fukumori, F.; Hogan, DA.; Sassanella, TM.; Kamagata, Y.; Takami, H.; Saari, RE. Microbial Diversity and Genetics of Biodegradation. Horikoshi, K.; Fukuda, M.; Kudo, T., editors. Japan Scientific Press; Tokyo: 1997. p. 35-51.
2. a Hutton JJ Jr. Tappel AL, Udenfriend S. Biochem. Biophys. Res. Commun. 1966; 24:179–184. [PubMed: 5965224] b Kivirikko KI, Myllyharju J. Matrix Biol. 1998; 16:357–368. [PubMed: 9524356] c Kershaw NJ, Caines MEC, Sleeman MC, Schofield CJ. Chem. Commun. 2005:4251–4263.

3. a Trewick SC, Henshaw TF, Hausinger RP, Lindahl T, Sedgwick B. Nature. 2002; 419:174–178. [PubMed: 12226667] b Falnes PØ, Johansen RF, Seeberg E. Nature. 2002; 419:178–182. [PubMed: 12226668]

4. a Ivan M, Kondo K, Yang H, Kim W, Valiando J, Ohh M, Salic A, Asara JM, Lane WS, Kaelin WG Jr. Science. 2001; 292:464–468. [PubMed: 11292862] b Jaakkola P, Mole DR, Tian YM, Wilson MI, Gielbert J, Gaskell SJ, von Kriegsheim A, Hebestreit HF, Mukherji M, Schofield CJ, Maxwell PH, Pugh CW, Ratcliffe PJ. Science. 2001; 292:468–472. [PubMed: 11292861] c Epstein ACR, Gleadle JM, McNeill LA, Hewitson KS, Rourke JO, Mole DR, Mukherji M, Metzen E, Wilson MI, Dhanda A, Tian Y-M, Masson N, Hamilton DL, Jaakkola P, Barstead R, Hodgkin J, Maxwell PH, Pugh CW, Schofield CJ, Ratcliffe PJ. Cell. 2001; 107:43–54. [PubMed: 11595184] d Bruick RK, McKnight SL. Science. 2001; 294:1337–1340. [PubMed: 11598268] e Yu F, White SB, Zhao Q, Lee FS. Proc. Natl. Acad. Sci. USA. 2001; 98:9630–9635. [PubMed: 11504942] f Masson N, Willam C, Maxwell PH, Pugh CW, Ratcliffe PJ. EMBO J. 2001; 20:5197–5206. [PubMed: 11566883] g Lando D, Peet DJ, Whelan DA, Gorman JJ, Whitelaw ML. Science. 2002; 295:858–861. [PubMed: 11823643] h Hewitson KS, McNeill LA, Riordan MV, Tian YM, Bullock AN, Welford RW, Elkins JM, Oldham NJ, Bhattacharya S, Gleadle JM, Ratcliffe PJ, Pugh CW, Schofield CJ. J. Biol. Chem. 2002; 277:26351–26355. [PubMed: 12042299]

5. a Tsukada, Y.-i.; Fang, J.; Erdjument-Bromage, H.; Warren, ME.; Borchers, CH.; Tempst, P.; Zhang, Y. Nature. 2006; 439:811–8163. [PubMed: 16362057] b Cloos PAC, Christensen J, Agger K, Maiolica A, Rappsilber J, Antal T, Hansen KH, Helin K. Nature. 2006; 442:307–311. [PubMed: 16732293] c Klose RJ, Yamane K, Bae Y, Zhang D, Erdjument-Bromage H, Tempst P, Wong J, Zhang Y. Nature. 2006; 442:312–316. [PubMed: 16732292]

6. Bollinger JM Jr. Price JC, Hoffart LM, Barr EW, Krebs C. Eur. J. Inorg. Chem. 2005:4245–4254.

7. van der Ploeg JR, Weiss MA, Saller E, Nahimoto H, Saito N, Kertesz, Leisinger T. J. Bacteriol. 1996; 178:5438–5446. [PubMed: 8808933]

8. Hanauske-Abel HM, G nzler V. J. Theor. Biol. 1982; 94:421–455. [PubMed: 6281585]

9. Groves JT, McClusky GA. J. Am. Chem. Soc. 1976; 98:859–861.

10. a Pavel EG, Zhou J, Busby RW, Gunsior M, Townsend CA, Solomon EI. J. Am. Chem. Soc. 1998; 120:743–753.b Zhou J, Kelly WL, Bachmann BO, Gunsior M, Townsend CA, Solomon EI. J. Am. Chem. Soc. 2001; 123:7388–7398. [PubMed: 11472170] c Neidig ML, Brown CD, Light KM, Fujimori DG, Nolan EM, Price JC, Barr EW, Bollinger JM Jr. Krebs C, Walsh CT, Solomon EI. J. Am. Chem. Soc. 2007; 129:14224–14231. [PubMed: 17967013]

11. a Zhang Z, Ren J, Stammers DK, Baldwin JE, Harlos K, Schofield CJ. Nat. Struct. Biol. 2000; 7:127–133. [PubMed: 10655615] b Elkins JM, Ryle MJ, Clifton IJ, Hotopp JCD, Lloyd JS, Burzlaff NI, Baldwin JE, Hausinger RP, Roach PL. Biochemistry. 2002; 41:5185–5192. [PubMed: 11955067]

12. a Price JC, Barr EW, Tirupati B, Bollinger JM Jr. Krebs C. Biochemistry. 2003; 42:7497–7508. [PubMed: 12809506] b Krebs C, Price JC, Baldwin J, Saleh L, Green MT, Bollinger JM Jr. Inorg. Chem. 2005; 44:742–757. [PubMed: 15859243]

13. a Price JC, Barr EW, Glass TE, Krebs C, Bollinger JM Jr. J. Am. Chem. Soc. 2003; 125:13008–13009. [PubMed: 14570457] b Bollinger JM Jr. Krebs C. J. Inorg. Biochem. 2006; 100:586–605. [PubMed: 16513177]

14. a Proshlyakov DA, Henshaw TF, Monterosso GR, Ryle MJ, Hausinger RP. J. Am. Chem. Soc. 2004; 126:1022–1023. [PubMed: 14746461] b Grzyska PK, Appelman EH, Hausinger RP, Proshlyakov DA. Proc. Natl. Acad. Sci. USA. 2010; 107:3982–3987. [PubMed: 20147623]

15. Riggs-Gelasco PJ, Price JC, Guyer RB, Brehm JH, Barr EW, Bollinger JM Jr. Krebs C. J. Am. Chem. Soc. 2004; 126:8108–8109. [PubMed: 15225039]

16. Sinnecker S, Svensen N, Barr EW, Ye S, Bollinger JM Jr. Neese F, Krebs C. J. Am. Chem. Soc. 2007; 129:6168–6179. [PubMed: 17451240]

17. a Hoffart LM, Barr EW, Guyer RB, Bollinger JM Jr. Krebs C. Proc. Natl. Acad. Sci. USA. 2006; 103:14738–14743. [PubMed: 17003127] b Eser BE, Barr EW, Frantom PA, Saleh L, Bollinger JM Jr. Krebs C, Fitzpatrick PF. J. Am. Chem. Soc. 2007; 129:11334–11335. [PubMed: 17715926] c Galonić DP, Barr EW, Walsh CT, Bollinger JM Jr. Krebs C. Nat. Chem. Biol. 2007; 3:113–116. [PubMed: 17220900] d Galonić DP, Barr EW, Matthews ML, Koch GM, Yonce JR, Walsh CT, Bollinger JM Jr. Krebs C, Riggs-Gelasco PJ. J. Am. Chem. Soc. 2007; 129:13408–13409.

[PubMed: 17939667] e Matthews ML, Krest CM, Barr EW, Vaillancourt FH, Walsh CT, Green MT, Krebs C, Bollinger JM Jr. Biochemistry. 2009; 48:4331–4343. [PubMed: 19245217] f Matthews ML, Neumann CS, Miles LA, Grove TL, Booker SJ, Krebs C, Walsh CT, Bollinger JM Jr. Proc. Natl. Acad. Sci. USA. 2009; 106:17723–17728. [PubMed: 19815524]

18. Price JC, Barr EW, Hoffart LM, Krebs C, Bollinger JM Jr. Biochemistry. 2005; 44:8138–8147. [PubMed: 15924433]
19. a Hegg EL, Ho RYN, Que L Jr. J. Am. Chem. Soc. 1999; 121:1972–1973.b Mehn MP, Fujisawa K, Hegg EL, Que L Jr. J. Am. Chem. Soc. 2003; 125:7828–7842. [PubMed: 12823001] c Mukherjee A, Marin-ho M, Bominaar EL, Münck E, Que L Jr. Angew. Chem. 2009; 121:1812–1815.
20. a Chiou Y-M, Que L Jr. J. Am. Chem. Soc. 1992; 114:7567–7568.b Chiou Y-M, Que L Jr. J. Am. Chem. Soc. 1995; 117:3999–4013.
21. Hollenhorst MA, Bumpus SB, Matthews ML, Bollinger JM Jr. Kelleher NL, Walsh CT. J. Am. Chem. Soc. 2010; 132:15773–15781. [PubMed: 20945916]
22. Neidig ML, Decker A, Choroba OW, Huang F, Kavana M, Moran GR, Spencer JB, Solomon EI. Proc. Natl. Acad. Sci. USA. 2006; 103:12966–12973. [PubMed: 16920789]
23. Fitzpatrick, PF. Adv. Enzymol. Relat. Areas Mol. Biol. Purich, DL., editor. Wiley; 2000. p. 235-294.
24. a Que L Jr. Acc. Chem. Res. 2007; 40:493–500. [PubMed: 17595051] b Nam W. Acc. Chem. Res. 2007; 40:522–531. [PubMed: 17469792]
25. a England J, Martinho M, Farquhar ER, Frisch JR, Bominaar EL, Münck E, Que L Jr. Angew. Chem. 2009; 121:3676–3680.Angew. Chem. Int. Ed. 2009; 48:3622–3626.b England J, Guo Y, Farquhar ER, Young VG Jr. Münck E, Que L Jr. J. Am. Chem. Soc. 2010; 132:8635–8644. [PubMed: 20568768] c Hendrich MP, Lacy DC, Gupta R, Stone KL, Greaves J, Ziller JW, Borovik AS. J. Am. Chem. Soc. 2010; 132:12188–12190. [PubMed: 20704272] d England J, Guo Y, Van Heuvelen KM, Cranswick MA, Rohde GT, Bominaar EL, Münck E, Que L Jr. J. Am. Chem. Soc. 2011; 133:11880–11883. [PubMed: 21739994]
26. a Borowski T, Bassan A, Siegbahn PEM. Chem. Eur. J. 2004; 10:1031–1041. [PubMed: 14978830] b Borowski T, Bassan A, Siegbahn PEM. Biochemistry. 2004; 43:12331–12342. [PubMed: 15379572] c Borowski T, Bassan A, Siegbahn PEM. Inorg. Chem. 2004; 43:3277–3291. [PubMed: 15132638] d de Visser SP. Chem. Commun. 2007:171–173.e Diebold AR, Brown-Marshall CD, Neidig ML, Brownlee JM, Moran GR, Solomon EI. J. Am. Chem. Soc. 2011; 133:18148–18160. [PubMed: 21981763]
27. a Angeli C, Cimiraglia R, Evangelisti S, Leininger T, Malrieu JP. J. Chem. Phys. 2001; 114:10252–10264.b Angeli C, Cimiraglia R, Malrieu JP. J. Chem. Phys. 2002; 117:9138–9153.
28. Kumar D, Thiel W, de Visser SP. J. Am. Chem. Soc. 2011; 133:3869–3882. [PubMed: 21344861]
29. Wirstam M, Lippard SJ, Friesner RA. J. Am. Chem. Soc. 2003; 125:3980–3987. [PubMed: 12656634]
30. Battino, R. Oxygen and Ozone. Pergamon press; New York: 1981.
31. a Kryatov SV, Rybak-Akimova EV, MacMurdo VL, Que L Jr. Inorg. Chem. 2001; 40:2220–2228. [PubMed: 11327894] b Lloyd CR, Eyring EM, Ellis WR Jr. J. Am. Chem. Soc. 1995; 117:11993–11994.c Feig AL, Becker M, Schindler S, van Eldik R, Lippard SJ. Inorg. Chem. 1996; 35:2590–2601. [PubMed: 11666474] d Costas M, Cady CW, Kryatov SV, Ray M, Ryan MJ, Rybak-Akimova EV, Que L Jr. Inorg. Chem. 2003; 42:7519–7530. [PubMed: 14606847] e Herold S, Lippard SJ. J. Am. Chem. Soc. 1997; 119:145–156.f Shan X, Que L Jr. Proc. Natl. Acad. Sci U. S. A. 2005; 102:5340–5345. [PubMed: 15802473]
32. Neese F, Liakos DG, Ye S. J. Biol. Inorg. Chem. 2011; 16:821–829. [PubMed: 21541855]
33. Borowski T, Noack H, Radoń M, Zych K, Siegbahn PEM. J. Am. Chem. Soc. 2010; 132:12887–12898. [PubMed: 20738087]
34. Mbughuni MM, Chakrabarti M, Hayden JA, Bominaar EL, Hendrich MP, M nck E, Lipscomb JD. Proc. Natl. Acad. Sci. USA. 2010; 107:16788–16793. [PubMed: 20837547]
35. Zhang Z, Ren JS, Harlos K, McKinnon CH, Clifton IJ, Schofield CJ. FEBS Lett. 2002; 517:7–12. [PubMed: 12062399]

36. Ye S, Price JC, Barr EW, Green MT, Bollinger JM Jr. Krebs C, Neese F. J. Am. Chem. Soc. 2010; 132:4739–4751. [PubMed: 20218714]
37. Kovaleva EG, Lipscomb JD. Science. 2007; 316:453–457. [PubMed: 17446402]
38. M nck, E. Physical methods in Bioinorganic Chemistry. Que, L., editor. Univeristy Science Books; Sausalito, CA: 2000. p. 287-319.
39. a de Visser SP. J. Am. Chem. Soc. 2006; 128:9813–9824. [PubMed: 16866538] b Ye S, Neese F. Proc. Natl. Acad. Sci. USA. 2011; 108:1228–1233. [PubMed: 21220293]
40. Mirica LM, McCusker KPMJW, Liu H-W, Klinman JP. J. Am. Chem. Soc. 2008; 130:8122–8123. [PubMed: 18540575]
41. a Shaik S, de Visser SP, Ogliaro F, Schwarz H, Schrçder D. Curr. Opin. Chem. Biol. 2002; 6:556–567. [PubMed: 12413538] b Shaik S, Kumar D, de Visser SP, Altun A, Thiel W. Chem. Rev. 2005; 105:2279–2328. [PubMed: 15941215]
42. Neese, F. ORCA - an ab initio, Density Functional and Semiempirical Program Package Verson 2.8.2011. Universität Bonn; Bonn, Germany:
43. a Becke AD. J. Chem. Phys. 1993; 98:5648–5652.b Lee CT, Yang WT, Parr RG. Phys. Rev. B. 1988; 37:785–789.
44. Sch fer A, Huber C, Ahlrichs R. J. Chem. Phys. 1994; 100:5829–5835.
45. Sch fer A, Horn H, Ahlrichs R. J. Chem. Phys. 1992; 97:2571–2577.
46. Neese F, Olbrich G. Chem. Phys. Lett. 2002; 362:170–178.
47. a Eichkorn K, Treutler O, Ohm H, Häser M, Ahlrichs R. Chem. Phys. Lett. 1995; 242:652–660.b Eichkorn K, Weigend F, Treutler O, Ahlrichs R. Theor. Chem. Acc. 1997; 97:119–124.
48. Kirchner B, Wennmohs F, Ye S, Neese F. Curr. Opin. Chem. Biol. 2007; 11:134–141. [PubMed: 17349817]
49. Neese F. J. Phys. Chem. Solids. 2004; 65:781–785.
50. Neese F, Wennmohs F, Hansen A, Becker U. Chem. Phys. 2009; 356:98–109.
51. Klamt A, Schüürmann G. J. Chem. Soc. Perkin Trans. 1993; 2:799–805.
52. Siegbahn PEM. J. Biol. Inorg. Chem. 2006; 11:695–701. [PubMed: 16830147]
53. Neese F. J. Chem. Phys. 2003; 119:9428.

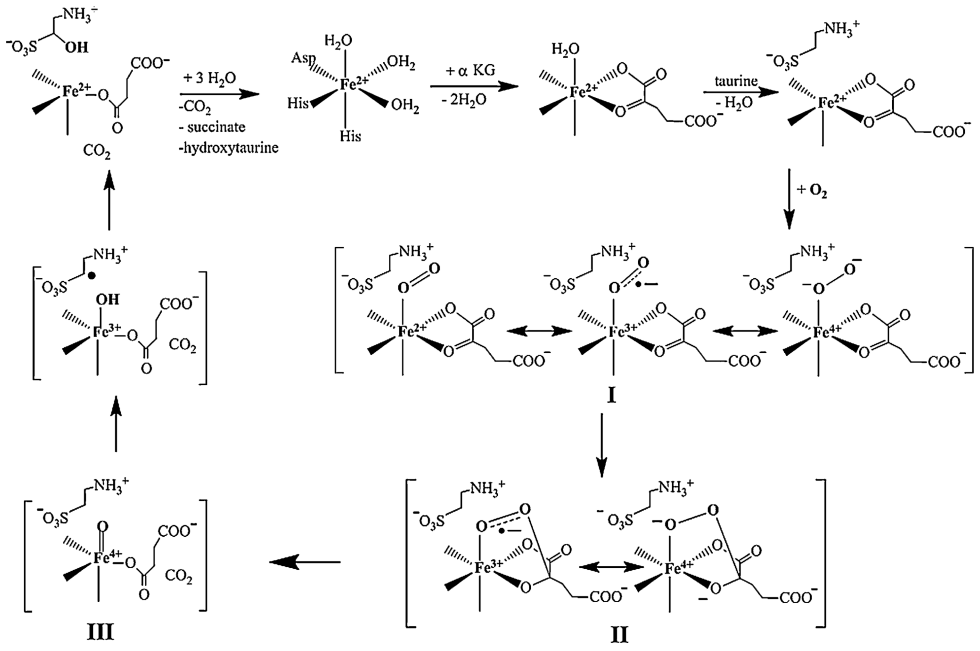

Scheme 1.
Proposed consensus mechanism of the Fe^{II}- and αKG-dependent dioxygenases.

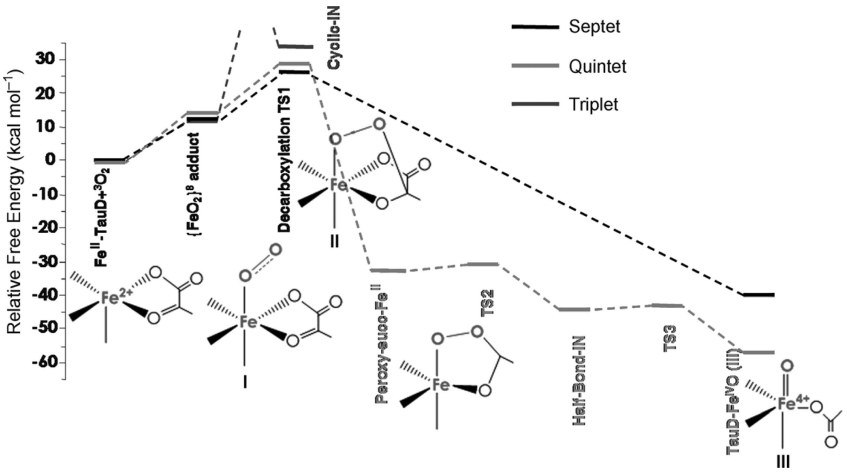

Figure 1.

The calculated potential-energy profile for the oxygen activation by the Fe^{II}- and αKG-dependent dioxygenases with the B3LYP density functional (**I, II, III** indicate the proposed intermediates in Scheme 1).

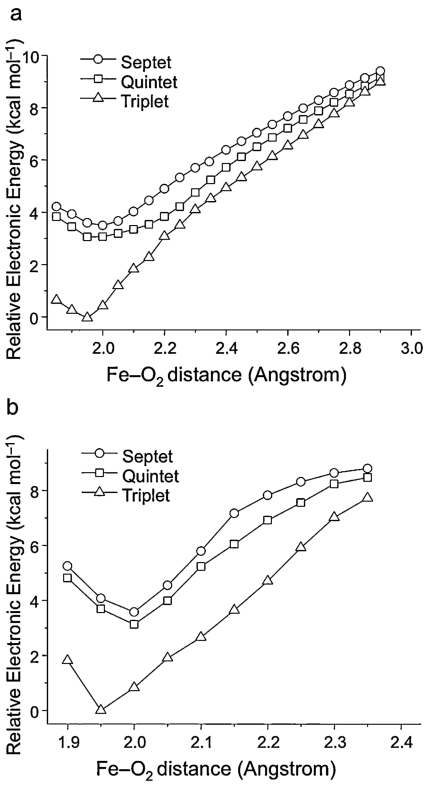

Figure 2.
The calculated O_2 binding as a function of the Fe–O_2 distances by using a) CASSCF and b) NEVPT2 methods.

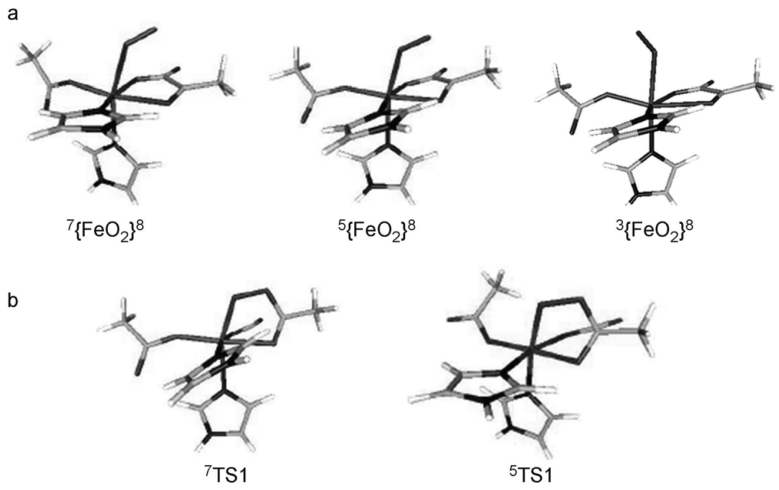

Figure 3.
The optimized geometries of a) the O_2 adducts on the septet, quintet, and triplet surfaces and b) the decarboxylation TS on the septet and quintet surfaces.

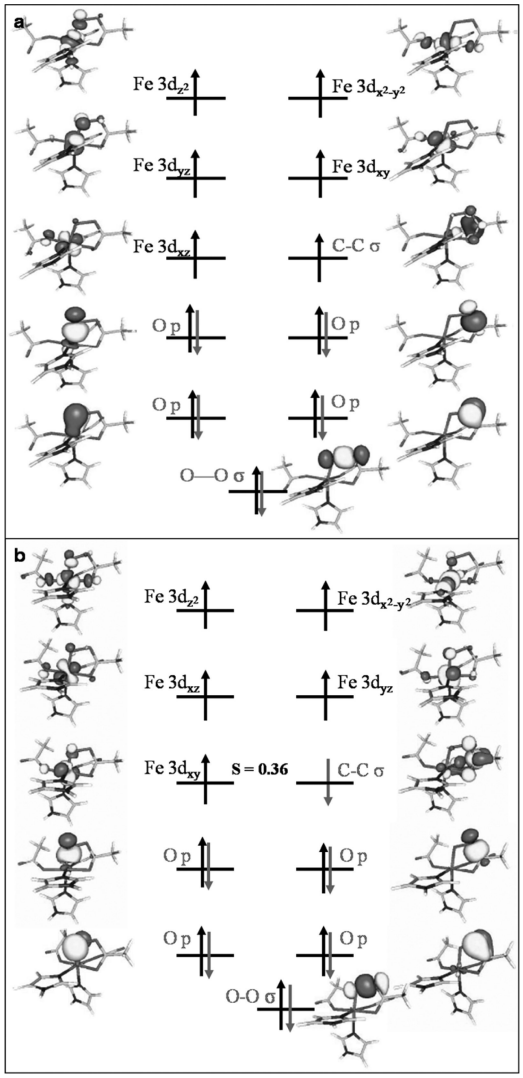

Figure 4.

Schematic MO diagram for a) ^{7}TS1 and b) ^{5}TS1. The spin-coupled pair represents unrestricted corresponding orbitals, whereas for the remaining orbitals quasi-restricted orbitals were employed.

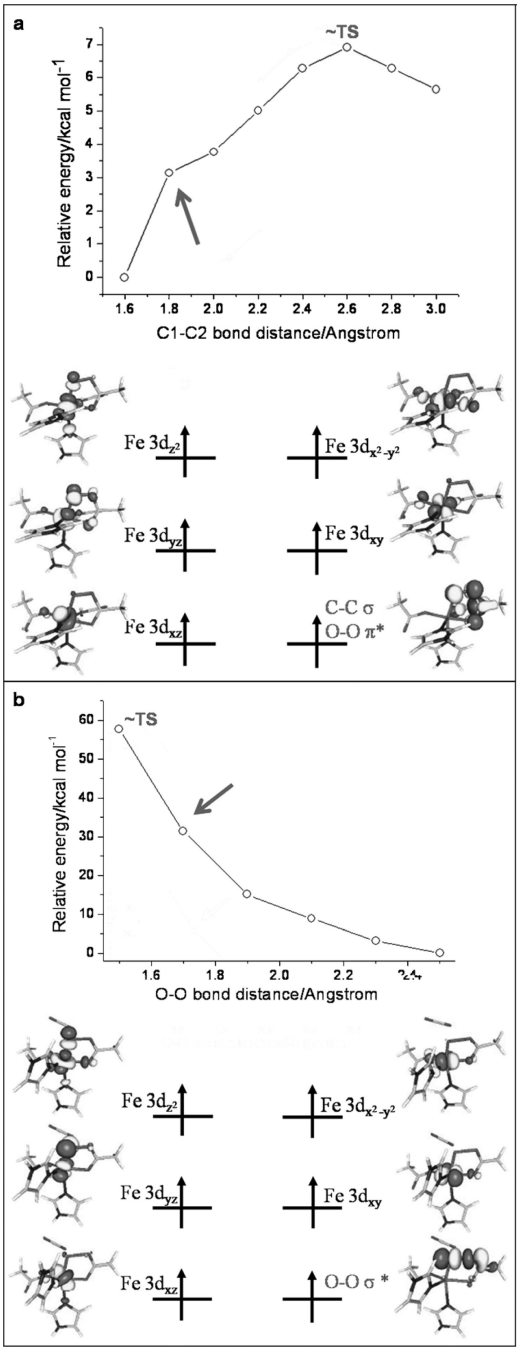

Figure 5.
Schematic MO diagrams for a) pre-^{7}TS1 and b) the decay of ^{7}TS1. Quasi-restricted orbitals were employed.

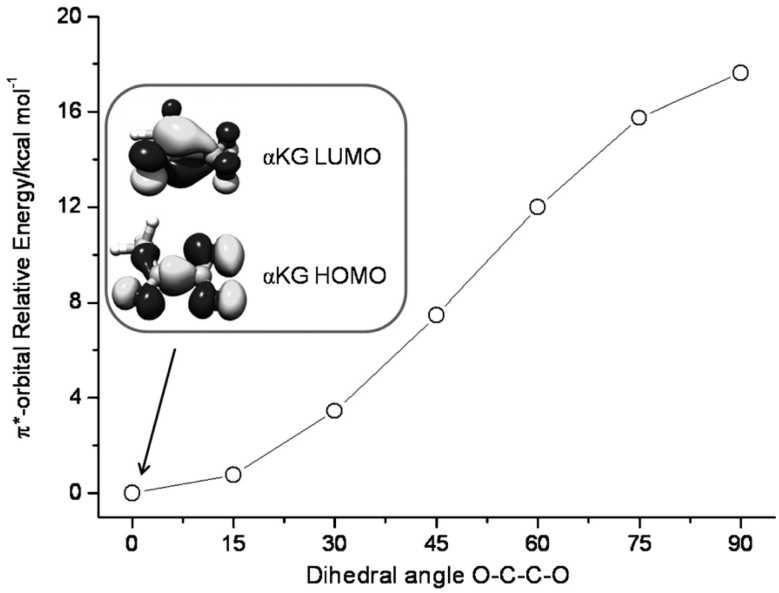

Figure 6.
Evolution of the energy of αKG LUMO as a function of the dihedral angle of O(carboxylate)-C1-C2-O(carbonyl).

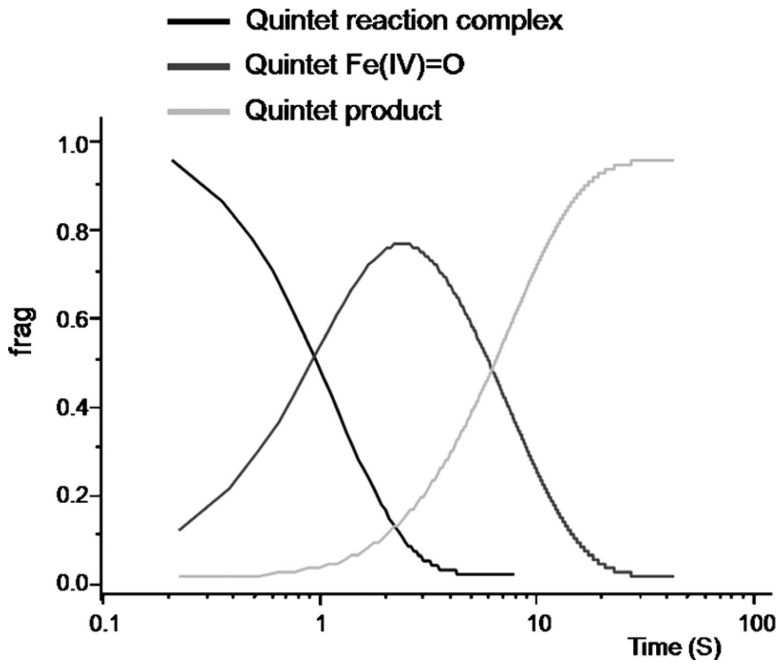

Figure 7.
The simulated kinetics at 273 K for the oxygen activation and C–H bond activation by TauD. For clarity, the intermediates that do not accumulate to more than 5% in the simulation are not shown in the figure.

Table 1

The calculated (B3LYP/def2-TZVPP) relative enthalpies and Gibbs free energies[a] [kcal mol^{-1}] for the catalytic cycle of oxygen activation of different spin states.

	Δ*H*	Δ*G*
septet O_2 adduct	3.1	12.6[b]
^{7}TS1	11.2	26.4
$^7(FeO)^{2+}$	–45.8	–40.0
quintet O_2 adduct	3.9	14.6[b]
^{5}TS1	12.0	28.5
quintet Fe^{II}-peroxosuccinate	–42.3	–32.3
$^5(FeO)^{2+}$	–61.8	–56.7
triplet O_2 adduct	2.6	12.2[b]
triplet bicyclic intermediate	14.5	31.0

[a] All energies reported here are relative enthalpies and Gibbs free energies computed with respect to the five-coordinate Fe^{II} complex and free triplet O_2.

[b] The addition of O_2 to the iron center of TauD was predicted to be endergonic by approximately 13 kcal mol^{-1}, which is mainly an entropic effect. As shown in the quantum mechanical/molecular mechanical (QM/MM) calculations on the O_2 binding to hemerythrin, van der Waals and electrostatic contribution from the protein environment amount to –10 $kcalmol^{-1}$ to the free energy.[29] Thus, if one takes these effects into account, the O_2 binding reaction in TauD is only slightly endergonic or isoenergetic given the error of the employed methodology.

Table 2

Comparison of the calculated relative electronic energies [kcal mol^{-1}] for the $\{FeO_2\}^8$ adducts with the different spin multiplicities using DFT B3LYP and ab initio CASSCF, NEVPT2, and CCSD(T) methods.

	B3LYP	CASSCF	NEVPT2	CCSD(T)
$^7\{FeO_2\}^8$	1.3	3.5	3.7	6.3
$^5\{FeO_2\}^8$	1.5	3.0	3.0	4.5
$^3\{FeO_2\}^8$	0	0	0	0

Table 3

The calculated relative free energies [kcalmol^{-1}] for the catalytic cycle of dioxygen activation of the different spin state using the simplified model.

	B3LYP	CCSD(T)
$^{7}\{FeO_2\}^{8}$	–0.2	1.5
$^{5}\{FeO_2\}^{8}$	0	0
^{7}TS1	9.9	5.4
^{5}TS1	9.9	no convergence[a]
$^{7}(FeO)^{2+}$	–59.4	–57.5
$^{5}(FeO)^{2+}$	–74.2	–83.6

[a] ^{5}TS1 should be nearly isoenergetic with ^{7}TS1 as indicated by its electronic structure.

Table 4

The key geometric parameters for the optimized geometries of the O_2 adducts on the septet, quintet, and triplet surfaces.

TauD-{FeO_2}^{8}	Septet	Quintet	Triplet
ΔE [kcalmol^{-1}]	0.4	1.1	0
Fe-O [Å]	2.317	2.110	2.298
O-O [Å]	1.247	1.289	1.260
Fe-O-O [°]	124.6	117.6	120.6
O(O_2)-C2 (αKG) [Å]	2.842	2.205	4.438
C1-C2 (αKG) [Å]	1.557	1.544	1.561
C2=O (carbonyl in αKG) [Å]	1.231	1.256	1.224
δ [mms^{-1}]	0.83	0.56	1.02
ΔE_Q [mms^{-1}]	0.91	–0.96	2.85

Table 5

Comparison of the geometric features of TS1 on the septet and quintet surface.

TS1	Septet	Quintet
Fe–O [Å]	1.961	2.043
O–O [Å]	1.434	1.367
Fe-O-O [°]	111.7	110.4
O(O2)–C2 (αKG) [Å]	1.340	1.455
C1–C2 (αKG) [Å]	2.549	1.721
C2–O (C=O in αKG) [Å]	1.557	1.317